Quantum-Mechanical Modeling of NBTI in High-k SiGe MOSFETs

Ph. Hehenberger*, W. Goes*, O. Baumgartner*, J. Franco°, B. Kaczer° and T. Grasser*
* Institute for Microelectronics, TU Wien, Gußhausstraße 27–29, A–1040 Wien, Austria ° IMEC, Leuven, Belgium
Email: {hehenberger|goes|baumgartner|grasser}@iue.tuwien.ac.at {francoj|kaczer}@imec.be

***Abstract*—Degradation and recovery of a multi-layer high-k SiGe pMOSFET due to the negative bias temperature instability (NBTI) is modeled on the basis of a refined non-radiative multi-phonon (NMP) theory. As the SiGe-layer forms a quantum-well inside the substrate, quantum mechanical effects like subbands are incorporated into the model. In combination with a distribution of defects featuring different energies, barrier heights, and positions inside the oxide, a large range of accelerated stress conditions can be very accurately described. The defects accounting for the recoverable part of the NBTI degradation are finally identified as switching traps.**

Keywords: NBTI, switching traps, non-radiative multi-phonon emission, high-k, quantum mechanical effects

I. Introduction

Over the last few years the number of scientific publications concerning the negative bias temperature instability (NBTI) has grown enormously. The associated controversies mostly covered the issue of the microscopic mechanism behind NBTI. The once popular reaction-diffusion model [1], [2] was eventually shown to be unable to describe the recovery after NBTI. For this reason other models have been developed, including charge trapping by either interface states and/or oxide traps [3]–[8]. The latest promising attempt to model the NBTI phenomenon is based on the non-radiative multi-phonon (NMP) theory after [9], [10]. It assumes the conservation of the total energy of the defect. The model has already been shown to successfully reproduce measurement data of small area devices containing only a few defects [11]. In this paper, large area devices are characterized and the quantum mechanical (QM) effects in these high-k SiGe MOSFETs are incorporated into the model.

II. Devices and Measurements

In order to reduce NBTI, buried SiGe channel p-MOSFETs with a thick SiGe quantum well of a high Ge-fraction ($55\,\%$) and a thin SiCap have been suggested [12], [13]. These devices, schematically depicted in Fig. 1, were subjected to NBTI-stress using various V_{str} and temperatures via the measure-stress-measure routine after [14]. For this, a static $I_{\mathrm{D}}(V_{\mathrm{G}})$-characteristic is taken first to obtain a reference of the threshold voltage. Then V_{G} is set to V_{str} for some specified time t_{s}, which causes the degradation. After stress, V_{G} is switched back close to the threshold voltage and the relaxation is monitored over time. Repeating this procedure with different stress times yields relaxation curves as depicted in Fig. 5. The degraded threshold voltage is monitored with a delay of $2\,\mathrm{ms}$.

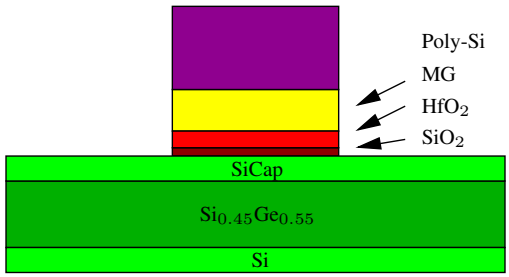

Fig. 1. Schematic view of the high-k gate-stack device including a thin SiCap and a high-mobility SiGe-layer as quantum well in the channel region to reduce NBTI [13]. The simulation is calibrated using $C(V)$-measurements and transfer characteristics.

III. Simulation

By using $C(V)$- and the previously mentioned $I_{\mathrm{D}}(V_{\mathrm{G}})$-characteristics, the proper layer thicknesses and their corresponding doping of the simulation were calibrated. To obtain the wavefunctions of the subbands in the channel of the MOSFET, the Schrödinger and Poisson equation were solved self-consistently using the Vienna Schrödinger Poisson solver (VSP2) [15]. The carrier concentration is calculated by treating the quasi-bound states as a two-dimensional electron gas with Fermi-Dirac distribution and the continuum states as 3D electron gas. The three X valley sorts of the conduction band as well as the heavy hole, light hole, and split off band are taken into account.

IV. Model

The non-radiative multi-phonon model of a switching oxide trap [11] is explained using a schematic configuration coordinate (CC) diagram for a single defect. The neutral defect state 1 and the charged defect state 2 are depicted in Fig. 2. Their corresponding metastable states $1'$ and $2'$ are separated by a thermal barrier from 1 respectively 2. The charge transfer reaction between state 1 and $2'$ under the applied electric field leads to a strong bias dependence of the barrier [11], [16]. The transitions from 1 to 2 and backwards are indicated by arrows, the corresponding reaction rates define the specific capture and emission time constants. Within these times the single defect is charged and discharged [11].

Because there is a large number of defects located in the oxide, a distribution of defects has to be assumed, with different relaxation energies, barrier heights, and positions

978-1-61284-418-3/11/$26.00 © 2011 IEEE

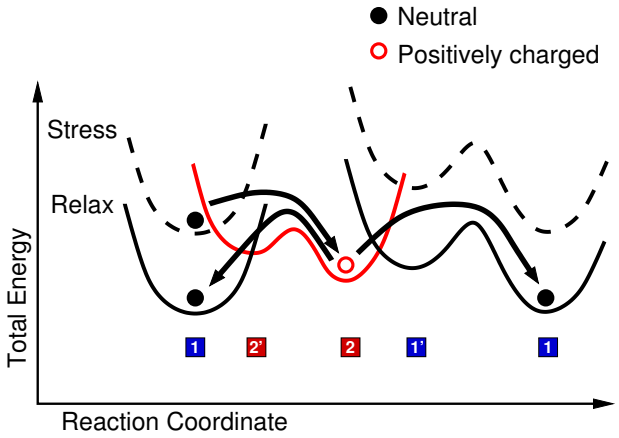

Fig. 2. Schematic configuration coordinate (CC) diagram model for a single defect. The different configurational potentials for each defect define the non-radiative multi-phonon process (NMP). The varying bias conditions (stress/relaxation) further change the relative position of the potentials and determine the transition rates from 1 to 2 (over the metastable $1'$ and $2'$) and back.

inside the oxide. As a reasonably discretization of the defect characteristics is inefficient, the defect properties are considered using a statistical approach.

Furthermore at different bias conditions during stress and relaxation for NBTI, only a part of all present defects is ever able to contribute to the degradation. That part of the contributing defects is marked within the defect band (cf. Fig. 4) being filled with 1000 representative different defects. These individual defects can now be charged and discharged repeatedly prior to annealing within the performed stress/relaxation cycles.

Instead of assuming all holes to be energetically located at the valence band edge of the substrate, we here distinguish the contributing subbands. For each subband the obtained transition rates determine the occupation of the individual defects at certain stress or relaxation times. These defect occupancies have then to be summed up over all subbands in order to finally determine the observable degradation. In the left of Fig. 3 the first five subbands are displayed based on their corresponding eigenenergies of which four are localized in the SiGe-layer. In the right of Fig. 3 the first two subbands are depicted for two stress and relaxation conditions. When switching from relaxation to stress the maxima of the subband wavefunctions move towards the interface, which raises the concentration of holes. The penetration of the wavefunctions is plotted on a log-scale to show the transmission probability. It can be clearly seen that the contribution of the subbands decreases with increasing order. As the bandbending inside the oxide due to the charged defects can be neglected, the WKB approximation is valid and used instead of the transition probability of the wavefunction.

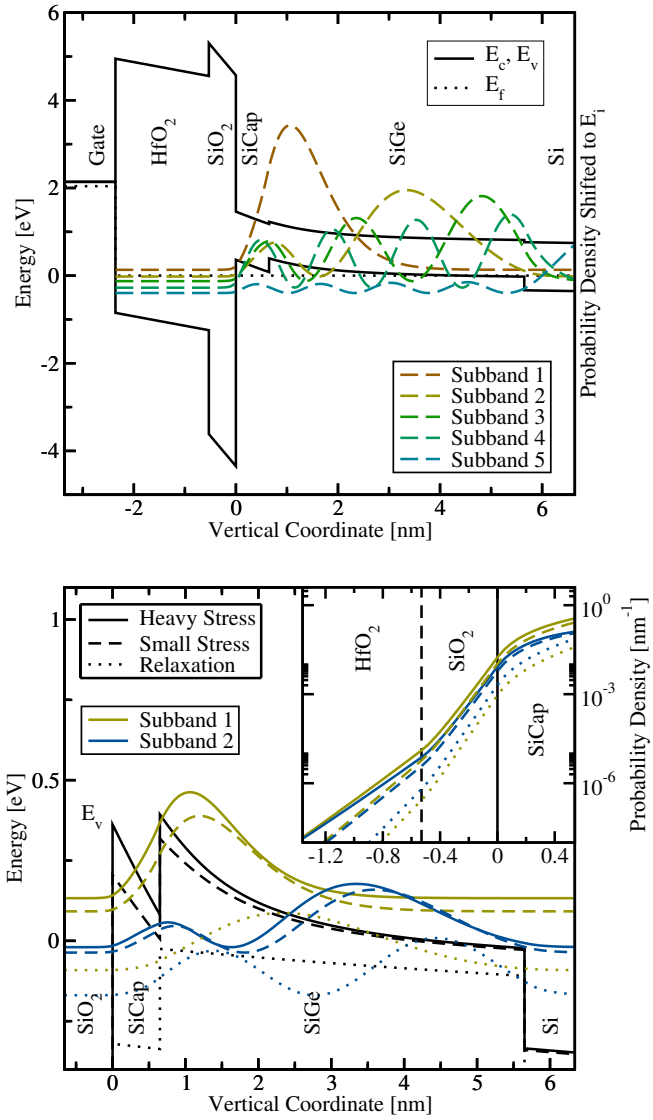

Fig. 3. **Left**: The NMP-rates are based on the different subbands serving as discrete provider of holes (shown for stress case). Only the first five subbands are displayed based on their corresponding eigenenergies of which four are localized in the SiGe-layer in the substrate. **Right**: When switching from relaxation to stress the maxima of the subbands move towards the interface, increasing the hole concentration. The inset shows the penetration of the wave function on a log-scale. The kink of the wave function in the oxide is caused by the layer structure.

V. Results

To validate the model, experimental data with logarithmically increasing stress times for different temperatures and V_{str} are essential. These measurement data are fitted using a single parameter set, which has to account for all measurements shown in this paper:

(1) For a given temperature and voltage, as illustrated in Fig. 5, it is possible to simulate a complex measurement-sequence, consisting of logarithmically increasing stress times, with very good agreement.

(2) The last relaxation sequence after more than 2000 s of

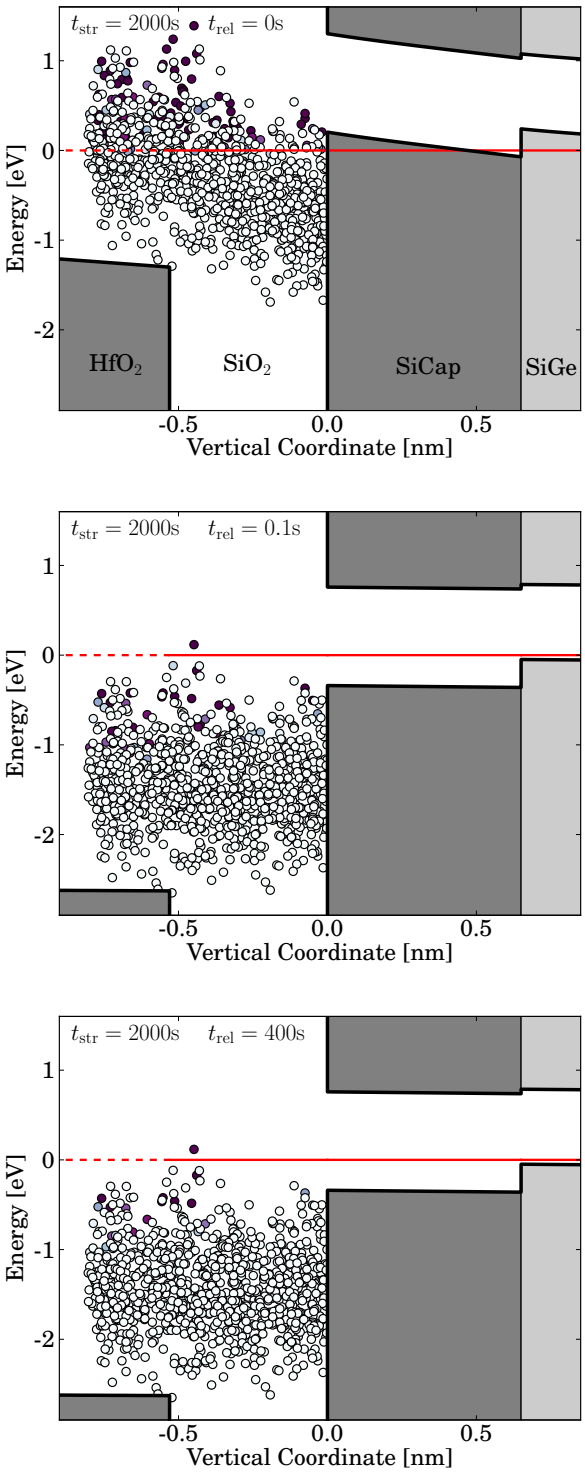

Fig. 4. The oxide defects are distributed over energy and depth and are marked filled when occupied. When switching from stress (**Top**) to relaxation (**Center** and **Bottom**) the defects are shifted downwards. The two graphs describe the last relaxation sequence for 125 °C and $V_{str} = 1.83$ V. **Top**: At the end of stress more than 9 % of the possible defects are filled. **Center**: After only 0.1 s of relaxation around 3 % of the defect are still filled. **Bottom**: After about 400 s relaxation only 1 % are left. This corresponds to nearly complete relaxation of the oxide traps. The permanent part left, see the bottom of Fig. 6, is due to depassivated interface states (the permanent component of the two-stage model [7]).

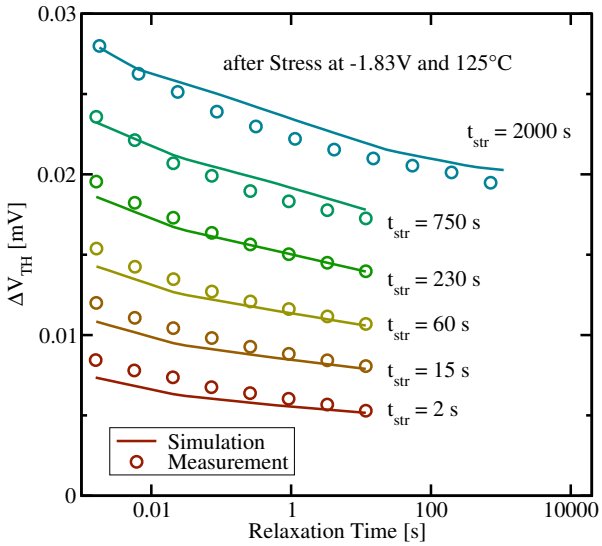

Fig. 5. The relaxation sequences of an measurement-sequence with logarithmically increasing stress times are plotted versus the simulation results. The same parameter set is applied for all simulations, yielding sound agreement.

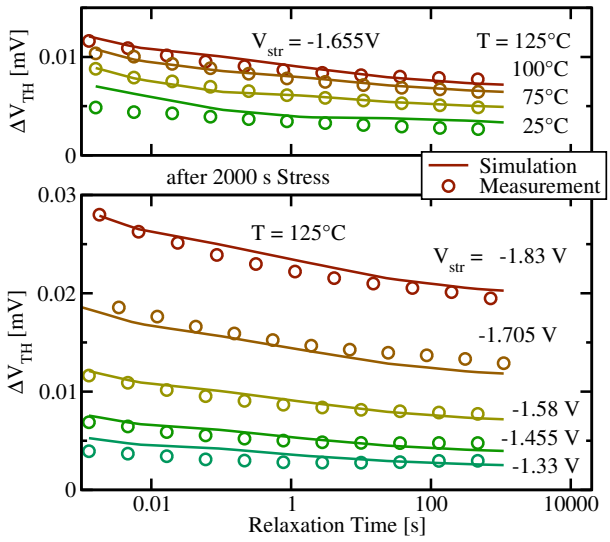

Fig. 6. The last relaxation sequence is depicted for different temperatures (**Top**) and stress voltages (**Bottom**). It can be clearly seen that the measurement is very well reproduced using our model.

stress is compared at different temperatures and for different stress voltages (Fig. 6). Despite device to device-deviations, as various MOSFETs have to be used for the measurements to avoid pre-stress, it can be clearly seen that the measurements are very well reproduced using the above described model.

(3) In Fig. 4 the percentage of the oxide defects occupancy is depicted for the last relaxation sequence for 125 °C and $V_{str} = 1.83$ V. At the beginning of the relaxation 9 % of the possible defects contribute, while after about 400 s relaxation only 1 % are left, which is equivalent to nearly complete relaxation of the switching traps.

(4) The permanent part left can be explained by the two-

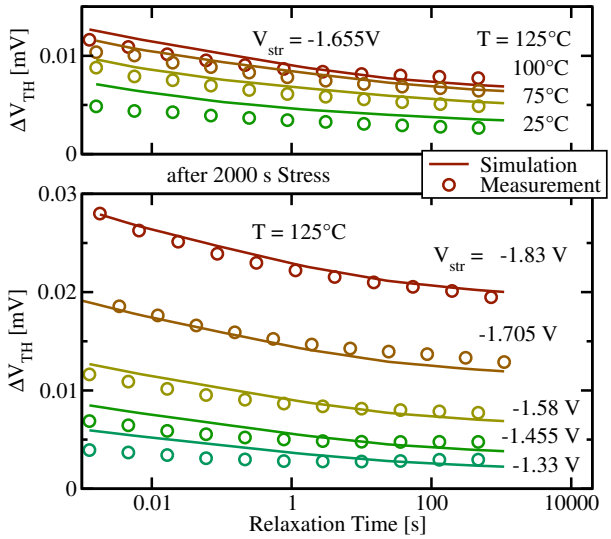

Fig. 7. The last relaxation sequence as depicted in Fig. 6 for different temperatures and stress voltages. When using 10000 instead of 1000 defects the simulation results become smoother. Although the simulation was performed with the same parameter set, the measurement is quite well reproduced using our model.

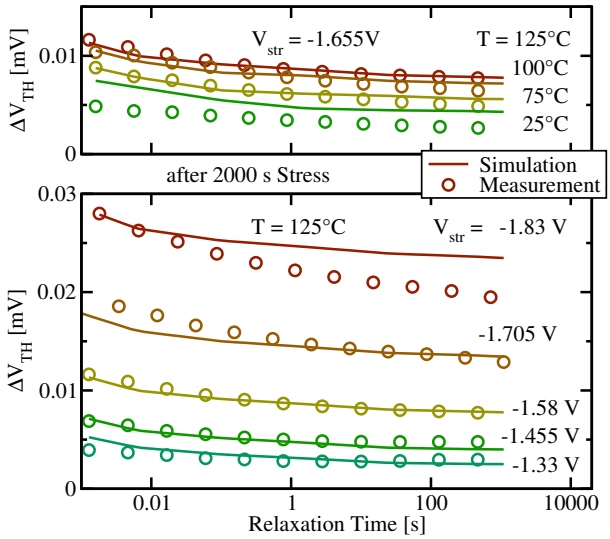

Fig. 8. The last relaxation sequence as depicted in Fig. 6 for different temperatures and stress voltages. The classical results assume all holes to be energetically located at the valence band edge of the substrate. Except for the heaviest stress conditions (125 °C and $V_{\mathrm{str}} = -1.705\,\mathrm{V}, -1.83\,\mathrm{V}$) the classical approach can as well be applied and yields rather good conformity to the experiment.

stage model [7] which assumes depassivated interface states contributing to NBTI (Fig. 6 bottom).

(5) The number of 1000 different defects exhibits a compromise between computational efforts and accuracy of the simulation which fits the experiments. When taking more defects the simulation results become smoother and do not contain the small kinks visible in Fig. 6. The simulation versus experimental results are depicted in the Fig. 7.

(6) The classical approach which assumes all holes to be energetically located at the valence band edge of the substrate shows small deviations from the QM-results, especially for 125 °C and $V_{\mathrm{str}} = -1.83\,\mathrm{V}$ (cf. Fig. 8). This is due to the missing influence of the subbands which are localized in the SiGe-layer.

VI. Conclusions

We have shown that NBTI degradation and recovery of a multi-layer high-k pMOSFET structure can be modeled on basis of a refined NMP theory which incorporates quantum mechanical effects like subbands. By repeatedly charging and discharging many distributed defects, the temporal occupation of the defects is obtained. The resultant simulation is fitted to measurement data covering a large range of accelerated stress conditions and yields excellent agreement. Additionally, the results of the classical approach are presented which lack in describing heavier stress conditions due to the missing influence of the bandbending inside the SiGe-layer.

VII. Acknowledgment

The imec core partners, the imec pilot line, and the imec Logic/DRAM program members are acknowledged for providing devices and experimental data.

References

[1] M. A. Alam, "A Critical Examination of the Mechanics of Dynamic NBTI for PMOSFETs," in *Proc. IEDM*, 2003, pp. 345–348.
[2] T. Grasser *et al.*, "Dispersive Transport and Negative Bias Temperature Instability: Boundary Conditions, Initial Conditions, and Transport Models," vol. 8, no. 1, pp. 79–97, 2008.
[3] A. Haggag *et al.*, "High-Performance Chip Reliability from Short-Time-Tests," in *Proc. IRPS*, 2001, pp. 271–279.
[4] V. Huard *et al.*, "NBTI Degradation: From Physical Mechanisms to Modelling," *Microel.Rel.*, vol. 46, no. 1, pp. 1–23, 2006.
[5] C. Shen *et al.*, "Characterization and Physical Origin of Fast Vth Transient in NBTI of pMOSFETs with SiON Dielectric," in *Proc. IEDM*, 2006, pp. 333–336.
[6] V. Huard *et al.*, "New Characterization and Modeling Approach for NBTI Degradation from Transistor to Product Level," in *Proc. IEDM*, 2007, pp. 797–800.
[7] T. Grasser *et al.*, "A Two-Stage Model for Negative Bias Temperature Instability," in *Proc. IRPS*, 2009, pp. 33–44.
[8] H. Reisinger *et al.*, "The Statistical Analysis of Individual Defects Constituting NBTI and its Implications for Modeling DC- and AC-Stress," in *Proc. IRPS*, 2010, pp. 7–15.
[9] K. Huang and A. Rhys, "Theory of Light Absorption and Non-Radiative Transitions in F-Centres," *Proc.R.Soc.A*, vol. 204, pp. 406–423, 1950.
[10] C. Henry and D. Lang, "Nonradiative Capture and Recombination by Multiphonon Emission in GaAs and GaP," *Phys.Rev.B*, vol. 15, no. 2, pp. 989–1016, 1977.
[11] T. Grasser *et al.*, "The Time Dependent Defect Spectroscopy (TDDS) for the Characterization of the Bias Temperature Instability," in *Proc. IRPS*, 2010, pp. 16–25.
[12] J. Franco *et al.*, "Improvements of NBTI Reliability in SiGe p-FETs," in *Proc. IRPS*, 2010, pp. 1082–1085.
[13] ——, "6å EOT $Si_{0.45}Ge_{0.55}$ pMOSFET with Optimized Reliability ($V_{DD} = 1\,V$): Meeting the NBTI Lifetime Target at Ultra-Thin EOT," in *Proc. IEDM*, 2010, pp. 70–73.
[14] B. Kaczer *et al.*, "Ubiquitous Relaxation in BTI Stressing New Evaluation and Insights," in *Proc. IRPS*, 2008, pp. 20–27.
[15] M. Karner *et al.*, "A Multi-Purpose Schrödinger-Poisson Solver for TCAD Applications," *J.Comp.Elec.*, vol. 6, no. 1-3, p. 179–182, 2007.
[16] W. Fowler *et al.*, "Hysteresis and Franck-Condon Relaxation in Insulator-Semiconductor Tunneling," *Phys.Rev.B*, vol. 41, no. 12, pp. 8313–8317, 1990.